

A potential new approach for preserving historical artifacts through gamma irradiation and green antimicrobials: Microbiological and theoretical screening

Ece Ergun^{a,*}, Hilal B.D. Halkman^a, Eren Kasımfirtına^b, Ömer Kantoğlu^a, Ümit Ergun^b, Ersin Orhan^b

^a Turkish Energy, Nuclear and Mineral Research Agency, Nuclear Energy Research Institute, Ankara, Türkiye

^b Department of Chemistry, Faculty of Arts and Sciences, Düzce University, 81620, Düzce, Türkiye

ARTICLE INFO

Handling editor: Piotr Ulanski

Keywords:

Ionizing radiation
Cultural heritage
Antimicrobial agents
Combined treatment
Density functional theory
Molecular docking

ABSTRACT

This study presents a novel combined treatment process for the decontamination of historical textiles, using gamma irradiation with green antimicrobial agents. Microbiological studies and theoretical approaches were utilized to investigate the effect of treatment processes individually and in combination on isolates from the textile museum. The mean D_{10} values and the required doses for complete inactivation were found to be 1.19 and 7.60 kGy for bacteria cocktail and 1.47 and 6.32 kGy for mold cocktail, respectively. The antimicrobial activities of two Schiff bases and their reduced derivatives were tested against gamma-resistant microorganisms by measuring the diameter of the inhibition zones. It was found that reduced derivatives exhibited higher antibacterial activity. All compounds were screened through an in-silico study to evaluate the physicochemical properties, drug-likeness, and toxicity profile. Molecular docking studies were performed to investigate the binding affinity of the title compounds against *E. coli* DNA gyrase B and topoisomerase IV. From the perspectives of both in vitro studies and computational analysis, L4 exhibited the highest biological activity. This finding revealed that the reduction of the imine bond and molecular flexibility have a significant influence on binding to the active site of the biomolecule. Finally, the combined treatment utilizing L4 with gamma irradiation demonstrated a synergistic effect, leading to a 2.6-fold reduction compared to the control, whereas the individual treatments of L4 and gamma irradiation exhibited approximately a 1-fold reduction. This synergistic effect presents an innovative approach to the historical artifact preservation, providing a more efficient and potentially safer decontamination strategy.

1. Introduction

Textiles are one of the oldest crafts recognized by humankind. These artifacts possess cultural, historical, and emotional significance, as they constitute integral components of the traditions and cultural heritage of communities and civilizations. Preserving this tangible wealth of humanity is important in terms of cultural value (Pandey et al., 2022). The primary cause of deterioration in historical textiles, similar to other artifacts, is the metabolic activities and nutritional requirements linked to the proliferation of living organisms. For instance, microbial growth on textiles can result in undesirable pigmentation. Bacteria, including *Brevibacterium*, *Bacillus*, *Rhodococcus*, *Corynebacterium*, *Achromobacter*, and *Streptomyces*, as well as fungi such as *Rhodotorula*, *Penicillium*,

Aspergillus, and *Cryptococcus*, are capable of synthesizing pigments in yellow, orange, brown, or black colors (Mazzoli et al., 2018; Gutarowska et al., 2017). Generally, bacteria such as *Cellulomonas*, *Cellvibrio*, *Clostridium*, *Cytophaga*, *Bacillus*, *Arthrobacter*, *Sporocytophaga*, *Microbispora*, *Pseudomonas*, *Nocardia*, and *Streptomyces* and fungi such as *Aspergillus*, *Verticillium*, *Penicillium*, *Mucor*, *Myrothecium*, *Trichoderma*, *Rhizopus*, *Alternaria*, *Fusarium*, *Aureobasidium*, and *Cladosporium* or their spores are responsible for the secretion of extracellular cellulolytic enzymes, resulting in the depolymerization of cellulose and degradation of plant-origin textile fibers (Branysova et al., 2022; Mazzoli et al., 2018; Szostak-Kotow, 2004). Keratin is the main constituent of wool, and keratinolytic bacteria (*Alcaligenes*, *Bacillus*, *Proteus*, *Pseudomonas*, and *Streptomyces*) and fungi (*Fusarium*, *Rhizopus*, *Aspergillus*, *Penicillium*,

* Corresponding author.

E-mail address: ergunlady@gmail.com (E. Ergun).

<https://doi.org/10.1016/j.radphyschem.2025.113247>

Received 15 May 2025; Received in revised form 4 August 2025; Accepted 15 August 2025

Available online 16 August 2025

0969-806X/© 2025 Elsevier Ltd. All rights are reserved, including those for text and data mining, AI training, and similar technologies.

Microsporium, *Chaetomium*, *Trichophyton*, and *Trichoderma*) are mainly responsible for the biodegradation of wool. In the case of silk, *Pseudomonas cepacia*, *Bacillus*, *Serratia*, *Pseudomonas*, and *Streptomyces* have been described as being able to modify the fibroin structure (Mazzoli et al., 2018; Szostak-Kotow, 2004; Forlani et al., 2000). On the other hand, some microorganisms, in particular *Staphylococcus* sp., *Aspergillus*, *Alternaria*, *Penicillium*, *Aureobasidium*, *Bacillus*, may act directly as human pathogens and may induce illnesses such as rhinitis, sinusitis, asthma, or alveolitis in humans (Russo and Palla, 2023; Di Carlo et al., 2016).

The extent and rate of degradation are influenced by the chemical and physical characteristics of the textile, environmental conditions, predominant microbial contaminants, and the interactions within the microbial community involved in the degradation process (Kavkler et al., 2015). Effective methods for addressing microorganism contamination and mitigating biodeterioration in museums and collections include controlling physical conditions, specifically through the establishment and maintenance of suitable temperature and relative humidity levels. In addition, mechanical, physical, and chemical methods are utilized for the conservation of artifacts. Among them, traditional procedures that employ biocidal products effectively eliminate microorganisms; however, some of them pose environmental and operator risks as they contain toxic substances and therefore do not offer a sustainable solution. Therefore, there is a necessity to develop innovative, sustainable, and safe methods and products (Cirone et al., 2023).

Radiation techniques have proven effective in the disinfection and preservation of cultural heritage artifacts, with national and international research programs establishing standardized methodologies for radiation treatment. Ionizing radiation, such as gamma rays, electrons, and X-rays, provides an effective method for eliminating microorganisms from cultural heritage artifacts (International Atomic Energy Agency, 2017). This technique is non-toxic and does not leave radioactive residues on objects. Ionizing radiation has the potential to cause genomic instability in living organisms by causing single-strand or double-strand breaks in the DNA of microorganisms by direct interaction, as well as damaging the sugar backbone and base pairs in DNA. These damages may lead to cellular death if not repaired (Danyo et al., 2024). Nevertheless, the sensitivity of microorganisms to high-energy radiation varies significantly among different types, species, and strains, each exhibiting distinct levels of radiosensitivity. The D_{10} value (decimal reducing dose) represents the radiation dose necessary to decrease a population by a factor of ten; on the other hand, the dose required to reduce the microbial load to a "blank level" (D_{BL}) is higher (Kantoglu et al., 2018). The levels and types of microorganisms within museums, archives, and libraries are variable (Skóra et al., 2015). As the exposure of artifacts to ionizing radiation aims to eradicate all strains of microorganisms or reduce the microbial load to a safety level, preparing a cocktail of microorganisms isolated from the artifacts and their storage and exhibition areas, along with calculating the D_{10} and D_{BL} values for this cocktail, is more practical for the radiation processing (Kantoglu et al., 2018).

The historical textiles mostly consist of natural fibers such as wool, linen, silk, and cotton and are dyed using natural organic colorants. It is important to note that ionizing radiation can degrade organic materials. The D_{10} and/or D_{BL} value may induce alterations in the molecular structure of organic fibers and particularly natural dyes utilized in historical textiles. Several studies have been conducted regarding the effect of gamma irradiation on the color of textiles. Chirila et al. (2018) investigated the effect of gamma irradiation at doses ranging from 5 to 40 kGy on the natural dyeing properties of linen and cotton textiles. The study revealed that cotton exhibited more saturated colors than flax fibers compared to unirradiated control samples, regardless of the applied dose (Chirila et al., 2018). Kavkler et al. (2018) reported that gamma irradiation of non-aged contemporary silk at an absorbed dose of 6 kGy resulted in no observable color change when compared to the untreated sample. The findings of another study indicated that gamma irradiation

at doses ranging from 0.5 to 25 kGy caused wool, linen, cotton, and silk fabrics to become more or less darker. It was reported that the change in darkness is more noticeable in samples dyed with natural colors (Vujcic et al., 2019). In this context, the use of a green antimicrobial agent combined with irradiation at lower doses could be employed as an alternative method in circumstances where the radiation doses applied are insufficient to eliminate the microorganisms and/or side effects have been identified in historical textiles. The efficacy of the combined treatments has been well documented in food preservation (Balaji et al., 2022; Begum et al., 2022; Ji et al., 2021, 2022; Shankar et al., 2022; Ben-Fadhel et al., 2021; Hossain et al., 2021; Robichaud et al., 2021; Zhang et al., 2020; Berdejo et al., 2019; Tawema et al., 2016). On the other hand, a study has examined the utilization of gamma irradiation and Ag and ZnO nanoparticles as a combined treatment of new cotton textile materials, and the antimicrobial activity of the treated textiles has been tested against only two bacterial strains (*Staphylococcus aureus* and *Pseudomonas aeruginosa*) (Capraru et al., 2022). Sakr et al. (2019) reported the use of a biocide (tricyclazole) before the irradiation at sub-lethal doses to inhibit melanin production by *S. canarius* found in the mural paintings. Abdel-Halim et al. (2013) proposed the use of gentamycin (antibiotic) with an irradiation treatment in order to eliminate *S. canarius* as an alternative method. Petushkova and Koestler (1996) investigated the bacterial decontamination of parchment and leather from archives and libraries of the former Soviet Union. They reported the effect of gamma irradiation in combination with two biocides (Preventol R-80 and Catamin AB). This study contributes to the existing literature as the first to investigate the combined effects of gamma irradiation and a green antimicrobial agent on the microbial cocktail isolated from the textile museum, rather than focusing on individual or a limited number of microbial strains.

Schiff bases are organic compounds containing an imine (azomethine) group ($>C=N-$) and are usually synthesized by the condensation of a carbonyl compound with a primary amine. They are used in various applications, including corrosion inhibition, catalysis, polymer stabilization, luminescence chemosensing, and as intermediates in organic synthesis. Schiff bases exhibit a wide array of biological activities, encompassing antibacterial, antifungal, and antiviral properties (Ceramella et al., 2022). Antibacterial drugs derived from Schiff bases exhibited notable efficacy against bacteria through structural modifications, whereas antifungal drugs primarily demonstrated effectiveness in treating skin diseases. Antiviral Schiff base drugs are presently utilized for the treatment of viral diseases, including influenza, herpes simplex, and HIV (Mushtaq et al., 2024). Due to the strong biological activities of Schiff bases, these compounds can be used to enhance the efficiency of the radiation treatment process.

The biological activities of molecules are essentially determined by their structure, physicochemical properties, and mechanisms of action. In-silico ADMET predictions refer to a new drug design approach that employs computational techniques to evaluate the potential drug-likeness and toxicity of proposed compounds by virtually screening extensive chemical databases (Darlami and Sharma, 2024). This approach offers a quick, cost-effective, and more comprehensive assessment. Molecular docking is a widely utilized and effective structure-based in-silico method for predicting the biological target-ligand interactions. This process typically involves predicting the molecular orientation of a ligand within a biological target, followed by estimating their binding affinity using a scoring function (Sahu et al., 2024; Pinzi and Rastelli, 2019).

In this study, the D_{10} and D_{BL} values of microorganisms isolated from the textile museum were determined. The use of two simple Schiff bases and their reduced derivatives as antimicrobial agents against gamma-resistant microorganism colonies was investigated. The ligands were screened through an in-silico study using the ADMET prediction tool to evaluate the structure-activity relationship and toxicity. In addition, molecular docking studies were also conducted to elucidate the differences in antimicrobial activities among the ligands and to investigate

their mode of action. DNA gyrase and topoisomerase IV were used in the molecular docking simulations due to their complementary functions in bacterial DNA metabolism and essential role in bacterial viability. Finally, the effect of the combined treatment of gamma irradiation and antimicrobial agent on inhibiting the bacteria cocktail was investigated. While existing methods for historic textile decontamination are generally based on single treatments, this study presents a new approach by evaluating the synergistic potential of a combined treatment using gamma irradiation with green antimicrobial agents.

2. Materials and methods

2.1. Sampling of microbial contamination and gamma irradiation

The sampling was carried out from the textile museum in Ankara, where folk costumes, shoes, socks, purses, lace, quilts, napkins, bundles, bedspreads, wedding dresses, carpets, and rugs collected from various regions of Anatolia are exhibited and preserved. Sterile cotton swabs were used to collect the microorganisms from the historical textile artifacts as well as cabinets and shelves in exhibition halls and storage rooms (Fig. S1). The samples were inoculated on tryptic soy agar (TSA) for bacteria and yeast extract glucose chloramphenicol (YGC) agar for mold. After inoculation, the bacterial plates were incubated at 28 °C for 48 h, and the mold plates were incubated at 28 °C for 72 h to obtain colonies (Fig. S2). Following the incubation period, a bacteria and a mold cocktail were prepared separately, and colony counts were performed. The suspensions of bacteria and mold cocktails (1 mL) were collected from the Petri dishes by washing with maximal recovery diluent (MRD, Merck) on a magnetic stirrer. The suspensions were subsequently transferred to sterilized Whatman paper (2 × 2 cm²) in individual sterilized Petri dishes. The samples were allowed to dry at ambient temperature for one night.

2.2. Gamma irradiation

A cobalt-60 irradiator (Ob-Servo Sanguis Co-60 irradiator, Hungary), located at the Nuclear Energy Research Institute in Ankara, Türkiye, was used to irradiate the bacteria and mold cocktail samples at doses of 0, 1, 3, and 5 kGy (dose rate: 1.2 kGy h⁻¹). The absorbed dose was determined using Harwell Gammachrome YR™ dosimeters (Chromwell, UK). Irradiation and microbiological analyses were performed in duplicate.

2.3. Determination of D_{10} and D_{BL} values

Subsequent to gamma irradiation, 0.2 g of Whatman paper was aseptically introduced into a sterile Erlenmeyer flask that contained 9.8 mL of MRD. The mixture was then agitated using a magnetic stirrer for 2 min. Serial dilutions with MRD were performed on the homogenized samples. One hundred microliters (μL) of the diluents were added to sterilized Petri dishes containing YGC agar and TSA, respectively. After inoculation, the YGC agar plates were incubated at 28 °C for 72 h, and the TSA plates were incubated at 28 °C for 48 h. Following incubation, the number of colonies was enumerated manually. The D_{10} value was determined from the slope of survivors (the number of colony-forming units per gram of sample, CFU mL⁻¹) versus the dose (kGy) plot. The D_{BL} value represented the dose at which the colony-forming unit was theoretically zero (the dose required to reduce the microbial load to a blank level).

2.4. Synthesis of Schiff bases and determination of antimicrobial activities

Bis-N,N'-(salicylidene)-1,3-propanediamine (L₁) and bis-N,N'-(salicylidene)-1,4-butanediamine (L₂) were prepared according to the reported procedures (Reglinski et al., 2002). In brief, L₁ and L₂ were synthesized via condensation reactions of salicylaldehyde (2 mol) with 1,3-propanediamine (1 mol) and 1,4-butanediamine (1 mol) in ethanol,

respectively. Following the isolation, these Schiff bases were reduced with sodium borohydride to obtain bis-N,N'-(2-hydroxybenzyl)-1,3-diaminopropane (L₃) and bis-N,N'-(2-hydroxybenzyl)-1,4-diaminobutane (L₄) (Ateş et al., 2010). Fig. 1 illustrates the molecular structures of the ligands.

The antimicrobial and antifungal activities of L₁, L₂, L₃, and L₄ against the gamma-ray-resistant bacterial and fungal colonies (the isolates after 5 kGy irradiation) were determined using the disk diffusion method. The sterilized filter paper discs impregnated with the synthesized molecules (5 mg mL⁻¹ in DMSO) were placed on tryptic soy agar and yeast extract glucose chloramphenicol agar seeded with the gamma-ray-resistant bacterial and fungal colonies. The plates for bacteria were incubated at 28 °C for 24 h, and the plates inoculated with mold were incubated at 28 °C for 72 h. Antibacterial activities were evaluated by measuring inhibition zone diameters generated by the ligands.

2.5. Theoretical studies

The physicochemically important properties, drug-likeness, and toxicity of the ligands were investigated using in silico-based computational prediction tools (ADMETlab version 2.0, <https://admetmesh.scbdd.com>). The drug-likeness properties of the title molecules were evaluated based on Lipinski's rule of five. The rule states that most "drug-like" molecules have logP ≤ 5, molecular weight ≤ 500, number of hydrogen bond acceptors ≤ 10, and number of hydrogen bond donors ≤ 5. Molecules violating one of these rules may have poor absorption or permeability (Lipinski et al., 1997).

The ORCA 5.0.2 software program was used to execute density functional theory (DFT) calculations to analyze the electronic properties of the compounds under investigation (Neese, 2022). The B3LYP functional was employed, and the def2-SVP (Split Valence Polarized) basis set was applied for preliminary structural optimizations, followed by the def2-TZVP (Triple Zeta Valence Polarized) basis set to enhance the accuracy of the optimization. Furthermore, D3BJ dispersion correction and RIJCOSX associated with complementary base sets were included in calculations (Grimme et al., 2010, 2011; Weigend, 2006; Weigend and Ahlrichs, 2005). A polarized continuum model (CPCM) was used to simulate the water phase to investigate solvation effects (Barone and Cossi, 1998). The coordinates of the optimized structures verified the absence of imaginary frequencies, remarking minimal energy conformations. The minimal energy coordinates of the compounds were presented in the supporting information (Tables S1–S8). Received output data were visualized, plotted, and rendered using Avogadro 1.95 and POV-Ray 3.7 (Hanwell et al., 2016; Hanwell et al., 2012; Persistence of Vision Raytracer Pty. Ltd., 2013a, 2013b).

The ground state energies calculated by DFT employing the B3LYP functional with the def2-TZVP basis set under water-phase were utilized to determine the electronic properties of the ligands. Molecular electrostatic potential (MEP) maps were generated for each title molecule along with Python scripts. The obtained maps were plotted utilizing Chimera (Pettersen et al., 2004).

For molecular docking studies, the crystal structures of E. coli DNA gyrase B complexed with ADP were sourced from the Protein Data Bank (PDB ID: 4PRV) at a resolution of 2.0 Å. The crystal structure of topoisomerase IV complexed with ADPNP was obtained (PDB ID: 1S16) at a resolution of 2.1 Å. These proteins were selected since they did not contain any missing residues in the active site (Stanger et al., 2014; Bellon et al., 2004). The crystal structures of proteins were prepared utilizing MGLTools 1.5.7, Swiss-PdbViewer, and BIOVIA Discovery Studio Visualizer (version 2024) following the removal of crystallized water molecules, ligands, and extra chains; only chain A was used in all proteins. Afterward, ligands obtained through DFT geometry optimization at ground state and proteins were converted into pdbqt format, which included polar hydrogen atoms and Kollman charges (Morris et al., 2009; Guex and Peitsch, 1997). The Autodock-GPU 1.6 docking software was used to identify the binding properties of the ligands to the

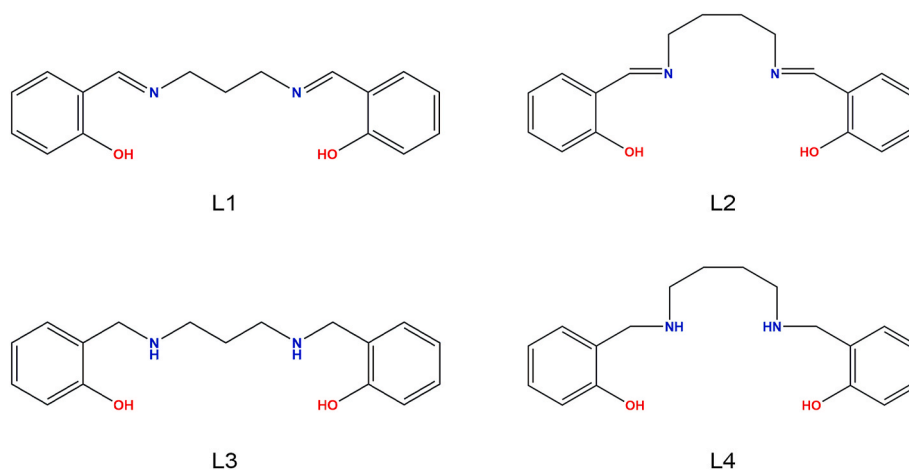


Fig. 1. Molecular structure of the synthesized Schiff bases (L1 and L2) and reduced derivatives (L3 and L4).

receptor (Santos-Martins et al., 2021). A flexible ligand–rigid receptor docking approach was applied to dock the ligands within the active site of the protein under investigation. All rotatable bonds of the ligands allowed full rotational flexibility, facilitating an extensive exploration of the conformational space within the rigid receptor binding site.

2.6. Combined effect of gamma irradiation and antibacterial formulation

The combined effect of gamma irradiation and antibacterial formulation was tested using L4, which exhibited the highest antibacterial activity among the investigated compounds. Five parallel plates were prepared using the spread plate method. The first plate was control without any treatment; the second plate was treated with antibacterial formulation alone; the third plate was treated with gamma irradiation alone; the fourth plate was treated with antibacterial formulation-gamma irradiation; the fifth plate was treated with gamma irradiation-antibacterial formulation. The samples were irradiated at a dose of 1.2 kGy (D_{10} value), and the antibacterial formulation was composed of L4 (5 mg mL^{-1}) in a water-ethanol (1:1, v/v) solvent. The samples were incubated at $28 \text{ }^\circ\text{C}$ for 24 h. Following incubation, the number of colonies was enumerated manually, and $\log \text{CFU mL}^{-1}$ was calculated.

3. Results and discussion

3.1. Determination of D_{10} , D_{BL} values, and antimicrobial activity of Schiff bases

Museums, as indoor venues, can be regarded as dynamic systems where particles of many origins are moved, transferred, and displaced between different environments. Microorganisms may enter museums through the bodies, clothing, and belongings of workers and visitors; indoor environmental sources such as contaminated floors and carpets

and malfunctioning ventilation systems; outdoor air via air vents, windows, doors, and other openings; or the introduction of contaminated artifacts or materials. This means that these external factors can cause additional infection, alongside the inherent microbial load of the artifact. In this context, the samples were collected using the cotton swab method from the textile artifacts and also any possible sources of contamination in this study. Initially, a bacteria and a mold cocktail were prepared, and microbial resistance to ionizing radiation of these cocktails was evaluated by determining D_{10} and D_{BL} values. Figs. 2 and 3, and Table 1 demonstrate the radiosensitivity of the bacteria and mold cocktails.

The D_{10} values were calculated using the linear regression equation of the curves illustrated in Figs. 2 and 3. The results presented in Table 1 show that the mean D_{10} value of the mold cocktail (1.47 kGy) is slightly higher compared to that obtained for the bacteria cocktail (1.19 kGy). On the other hand, the mold cocktail requires a mean dose of 6.32 kGy , while the bacteria cocktail needs a higher dose of 7.60 kGy for complete inactivation. This finding suggests that the bacteria cocktail involves the organism(s) that exhibit relative resistance to higher doses of ionizing radiation. Studies on the inactivation of certain microorganisms by ionizing radiation have been published in the literature. Li et al. (2025) indicated that doses exceeding 5, 7.5, and 15 kGy were required to prevent fungal colony formation for *A. flavus*, *A. niger*, and *A. versicolor*, respectively. Marušić et al. (2020) reported that the natural contamination of the investigated paper included *Aspergillus* spp., *Penicillium* spp., *Cladosporium* spp., unidentified white mycelia, and yeasts, which are commonly present on paper materials in libraries and archives. The findings demonstrated a decrease in the mycobiota after irradiation at a dose of 7 kGy . Another study reported that the D_{10} value and efficient dose for the reduction of mold cocktail isolated from the documents stored in the Ottoman Archives were 1 and 6 kGy , respectively (Kantoglu et al., 2018). An average dose of $8 \pm 2 \text{ kGy}$ and a maximum dose of 10 kGy were recommended as reference doses for overall

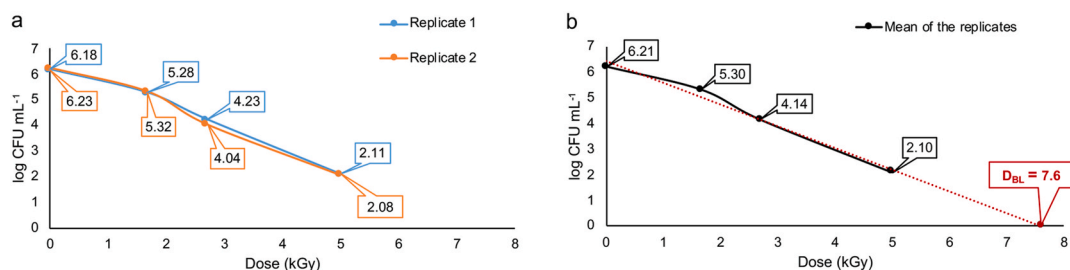


Fig. 2. Effect of gamma irradiation (0–5 kGy) on the bacteria cocktail a) replicates of bacterial count b) mean values of bacterial count. The concentration of viable bacterial counts was expressed as the logarithm of the number of colony-forming units per milliliter ($\log \text{CFU mL}^{-1}$).

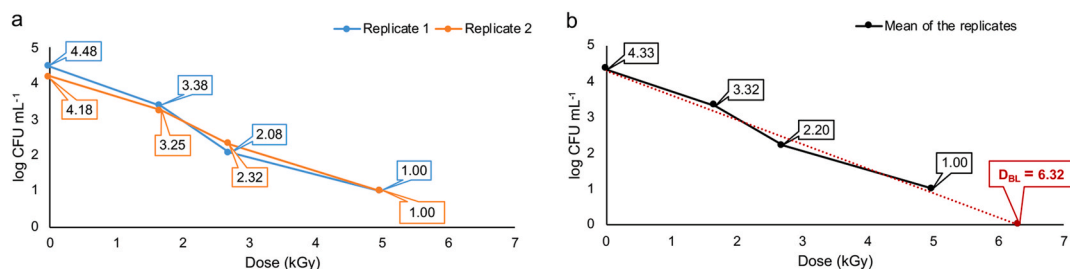


Fig. 3. Effect of gamma irradiation (0–5 kGy) on the mold cocktail a) replicates of mold count b) mean values of mold count. The concentration of viable mold counts was expressed as the logarithm of the number of colony-forming units per milliliter ($\log \text{CFU mL}^{-1}$).

Table 1
Radiosensitivity of the bacteria and mold cocktail.

		First Replicate	Second Replicate	Mean
Bacteria	^a RE	$y = -0.83x + 6.40$	$y = -0.85x + 6.42$	$y = -0.84x + 6.41$
	^b R ²	0.984	0.984	0.984
	^c DR	0.83	0.85	0.84
	^d D ₁₀ (kGy)	1.20	1.18	1.19
	^e D _{BL} (kGy)	7.68	7.51	7.60
	Mold	^a RE	$y = -0.71x + 4.41$	$y = -0.65x + 4.20$
^b R ²		0.969	0.993	0.983
^c DR		0.71	0.65	0.68
^d D ₁₀ (kGy)		1.41	1.54	1.47
^e D _{BL} (kGy)		6.21	6.46	6.32

^a Regression equation.

^b Correlation coefficient.

^c Death rate.

^d Decimal reducing dose.

^e Blank reducing dose.

disinfection of cultural heritage based on the side effects (Ponta et al., 2017). Abdel-Halim et al. (2013) examined the effect of gamma irradiation on isolated *Streptomyces*, revealing that *S. canarius* exhibited the highest resistance to gamma irradiation among the strains tested. This strain showed resistance up to 25 kGy, while *S. chibaensis* and *S. albidofuscus* demonstrated resistance to 20 kGy, and *S. ambofaciens* resisted up to 15 kGy. Resistance to gamma irradiation was lower (10 kGy) in the other strains.

The complete inactivation doses may adversely affect textile artifacts. The antimicrobial properties of the synthesized ligands (Fig. 1) were determined against gamma-resistant bacteria and mold colonies to evaluate their effectiveness in reducing the required decontamination doses. Antibacterial activity results were expressed in terms of the zone of inhibition (mm) (Table 2). No discernible zone of inhibition was observed for the compounds under investigation against the mold cocktail, indicating L1-L4 lack antifungal activity. On the other hand, all the ligands were found to be more or less effective against the bacteria cocktail (L4 > L3 > L2 > L1) based on measured inhibition zones ranging from 8.10 to 10.45 mm (Table 2). It was reported that the

Table 2
Antibacterial activities of the ligands (L1-L4).

Ligands	L1	L2	L3	L4
Inhibition zone diameter, mm (mean ± standard error)	8.10 ± 0.18	9.21 ± 0.11	10.13 ± 0.01	10.45 ± 0.04

synthesized four ONNO-type salophen Schiff bases showed antibacterial activity against two Gram-positive (*Staphylococcus aureus* and *Streptococcus pneumoniae*) and two Gram-negative (*Escherichia coli* and *Pseudomonas aeruginosa*) bacterial strains with a maximum 10 mm inhibition zone diameter (Gogoi and Barman, 2023). Kargar et al. (2022) investigated the antibacterial potential of two new ONNO-type salicylidene-based Schiff bases against two Gram-positive (*Staphylococcus aureus* and *Bacillus cereus*) and two Gram-negative (*Escherichia coli* and *Pseudomonas aeruginosa*) bacterial strains and reported that the inhibition zone diameters were in the range of 9–12 mm. The antibacterial activities of the two synthesized ONNO-type ligands were screened against *B. cereus*, *C. diphtheriae*, *E. coli*, *K. pneumoniae*, *P. mirabilis*, *P. aeruginosa*, *S. typhi*, *S. dysenteriae*, and *S. aureus* strains and ranged from 5 to 22 mm (Chohan et al., 2008). In our study, it was found that Schiff bases (L1 and L2) exhibited less activity (small and unclear inhibition zones, Table 2 and Fig. S3) compared to their reduced forms (L3 and L4). The observed activity of L3 and L4 probably arises from the higher flexibility and the presence of additional hydrogen atoms after the reduction of the imine group. These additional hydrogen atoms can enhance the formation of hydrogen bonds with the target cell constituents. These suggestions are in agreement with the previously reported studies (Oboňová et al., 2023; Sharma et al., 2011) and were also tested with in silico computational methods.

3.2. In silico physicochemical data and toxicity assessment of the ligands

In this study, computational approaches were used to predict the structure-activity relationship and toxicity of the ligands. Table 3 shows some in silico physicochemical data for L1-L4.

The Lipinski's rule of five (RO5) represents widely accepted guidelines for physicochemical properties, which an ideal drug molecule should satisfy. This indicator provides a prediction regarding the drug-likeness of a chemical compound with biological activity, specifically designed for oral administration (Ahmad et al., 2023). As can be seen in

Table 3
In silico physicochemical data of Schiff bases L1-L4.

^a Ls ^c	Rules of Lipinski					^d nRot	^e nRig	^f Flex
	^b MW	^c logP	^d nHD	^e nHA	^f nViol			
L1	282.14	3.41	2	4	0	6	14	0.43
L2	296.15	3.71	2	4	0	7	14	0.50
L3	286.17	1.13	4	4	0	8	12	0.67
L4	300.18	1.41	4	4	0	9	12	0.75

^a Ls: Ligands;

^b MW: Molecular weight;

^c logP: predicted octanol-water distribution coefficient;

^d nHD: Number of H bond donors;

^e nHA: Number of H bond acceptor;

^f nViol: Number of violation according to Lipinski's rule of five;

^g nRot: Number of rotatable bonds;

^h nRig: Number of rigid bonds;

ⁱ Flex: Flexibility (nRot/nRig)

Table 3, none of the title molecules violated Lipinski criteria (see Section 2.5), indicating these molecules have favorable absorption or permeability characteristics, making them suitable candidates for development as orally active drugs. However, this study focuses on the direct application of L1-L4 as antimicrobial agents targeting bacteria populations present on the cultural heritage artifacts. Consequently, these physicochemical features may also elucidate the difference in the antibacterial activity of L1-L4 observed experimentally. Therefore, the results of the physicochemical data of L1-L4 were interpreted in terms of ligand and target macromolecule interaction.

It was found that the reduction of the imine bond significantly decreased the hydrophobic nature of the Schiff bases ($\log P_{L1}$ and $\log P_{L2} > \log P_{L3}$ and $\log P_{L4}$). As the antibacterial activity of L3 and L4 was experimentally found to be higher than that of L1 and L2, it can be suggested that hydrophilic interaction with the target cell constituent is the driving force for bioactivity against the bacteria cocktail. The greater quantity of hydrogen bond donors (nHD_{L1} and $nHD_{L2} < nHD_{L3}$ and nHD_{L4}) appears to improve antibacterial activity, highlighting the importance of hydrogen bond interactions in bioactivity. These parameters indicate the significance of the single C–NH amine bond present in reduced derivatives for higher bioactivity (Oboňová et al., 2023).

The number of rigid bonds in L1 and L2 is higher compared to their reduced forms (L3 and L4). On the other hand, the number of rotatable bonds increases sequentially from L1 to L4. Accordingly, the predicted flexibility of the title molecules follows the order $Flex_{L1} < Flex_{L2} < Flex_{L3} < Flex_{L4}$, which correlates well with the experimental results of antibacterial activity. The higher flexibility of L4 may have allowed it to adopt a conformation that is complementary to the three-dimensional structure of the biological target (Caron et al., 2020). This flexibility may have contributed to the ligand–target interaction, which could be another reason for the higher antibacterial activity observed experimentally for L4.

In addition, it is essential to examine the potential health risks that these compounds may pose to museum personnel when applied as antibacterial agents on artifacts. Accordingly, the toxicity prediction data for the ligands are given in Tables S9–S11. From a toxicological standpoint, the data (Table S9) demonstrate that L3 and L4 are safer options (Xiong et al., 2021). The ADMETlab prediction indicates a significantly low probability of inducing mutagenicity (AMES Toxicity), acute toxicity, eye corrosion, and eye irritation for reduced derivatives in comparison to L1 and L2. However, L3 and L4 may be hepatotoxic agents due to the comparatively high probability of hepatotoxicity predicted by ADMETlab. The ADMET prediction indicates a significant risk of respiratory toxicity for all investigated compounds, necessitating the implementation of precautions during application. Tox21 is a toxicity assessment method to predict whether a certain chemical compound has the potential to disrupt processes in the human body that may lead to negative health effects (Richard et al., 2021). In the view of the Tox21 pathway, L1 and L2 could be toxic at high and moderate levels for NR-AhR, NR-Aromatase, NR-ER, NR-PPAR-gamma, SR-ARE, SR-A-TAD5, SR-HSE, SR-MMP, and SR-p53. On the other hand, L3 and L4 have no toxic effect for all the Tox21 pathways (Table S10). Finally, there are no warning signs related to the toxicophore rules for all ligands (Table S11). It can be concluded that L3 and L4 are safer options for utilization as antibacterial agents.

3.3. DFT calculations

Prior to molecular docking studies that will provide insights into the factors contributing to the different antibacterial activities observed experimentally, the molecular geometries of the title compounds were optimized for docking calculations. Based on the optimized geometry of the ligands, frontier molecular orbitals (HOMO-LUMO) and their energies, dipole moments, and molecular electrostatic potential (MEP) maps were also calculated to elucidate the electronic properties of the molecules.

The HOMO–LUMO distributions of the ligands with their HOMO–LUMO energy gap (ΔE) values are presented in Fig. S4 and S5. The HOMO indicates the electron-donating ability, whereas the LUMO defines an electron-accepting capability of a molecule (Bhatia, 2024). The stability and intramolecular charge transfer potential of a molecule are significantly influenced by the HOMO–LUMO energy gap (Musatut et al., 2024; Tanvir et al., 2024). Based on the obtained results in the aqueous phase, the ΔE values for L1 (4.61 eV) and L2 (4.73 eV) were found to be less than those of their reduced counterparts, L3 (5.707 eV) and L4 (5.708 eV). These findings indicate that L3 and L4 exhibit higher chemical stability and are less susceptible to intramolecular electron transfer from HOMO to LUMO. On the other hand, L1 and L2, with lower ΔE values, possess greater intramolecular charge transfer character. This intramolecular interaction may be one of the reasons for the low antibacterial activity of L1 and L2, decreasing the electron density in the binding sites with the target protein.

When a ligand approaches a receptor closely, it can diffuse and dock to the binding site on the biomolecule. The initial phase of this process may be facilitated by long-range electrostatic interactions between the ligand and the receptor, subsequently strengthened by short-range hydrogen bonds and van der Waals interactions (Schaeffer, 2008). In addition to charged molecules, ligands having permanent dipoles can also undergo electrostatic interactions, which can result in dipole-dipole interactions. Moreover, a ligand possessing a permanent dipole can induce a dipole in the active site of the receptor. The strength of these interactions is contingent upon the dipole moments of the molecules. Therefore, dipole moment is one of the most suitable parameters for characterizing the ligand-biomolecule interactions. The dipole moments of the ligands in Debye (D) increase in the following order: L1 (7.170 D), L2 (7.200 D), L3 (7.980 D), and L4 (8.950 D), which is consistent with the observed antibacterial activity results. The relatively higher dipole moment of reduced ligands, particularly L4, may be the driving force for their interaction with the target by facilitating their diffusion into the biomolecule.

MEP plots were used to analyze the electron-rich and electron-deficient parts of the molecules, which aids in the prediction of active sites for hydrogen bonding interactions (Akbari et al., 2024). Different electrostatic potential values on the surface of the molecules are represented by different colors. The blue color indicates the electron-poor regions acting as hydrogen bond donors, while the red color denotes the electron-rich regions serving as hydrogen bond acceptors (Storer and Hunter, 2022). Fig. 4 illustrates that all ligands have a non-uniform (asymmetrical) charge distribution, and this asymmetrical charge distribution is more pronounced in L3 and L4. The ligands display a partial

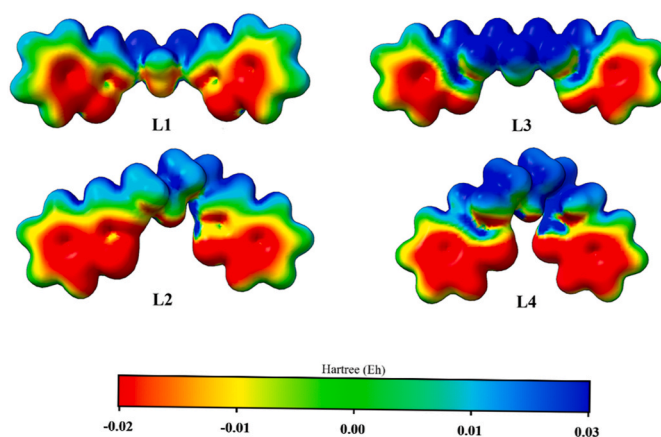


Fig. 4. Molecular electrostatic potential (MEP) $V(r)$ illustration of the title compounds calculated using B3LYP functional with the def2-TZVP basis set under water-phase. Blue indicates the electron-deficient and red indicates the electron-rich regions. (For interpretation of the references to color in this figure legend, the reader is referred to the Web version of this article.)

positive charged region (blue) predominantly at the center (alkyl chain). The partial negative charged region (red) is located around the hydroxyl sites of the aromatic rings for all molecules. However, L1 and L2 possess a larger red region over hydroxyl oxygen and nitrogen, which can be predicted as a characteristic O-H...N intramolecular hydrogen bond interaction (Filarowski et al., 1999). This intramolecular hydrogen transfer may have reduced the hydrogen-accepting capability of the oxygen and nitrogen atoms in the ligands, leading to a reduction in the ligand-biomolecule interaction. In the case of L3 and L4, on the other hand, the electron density (red color) remains on the hydroxyl groups, indicating that these groups maintain their hydrogen-accepting capacity. However, the blue color has become brighter, showing that the reduction of the imine bond has decreased electron density in that region. The gaining of an additional hydrogen atom due to the reduction has increased the ability of the molecules to donate hydrogen bonds, which is probably one of the main reasons for enhanced bacterial activity, as discussed in Section 3.2.

3.4. Molecular docking studies

Molecular docking is a computational technique that plays a key role in drug discovery and determining the biological activity of compounds. It involves predicting atomic-level interactions between ligands and target proteins (Agu et al., 2023; Roney et al., 2023). This study carried out a comprehensive docking investigation to clarify the binding interactions, conformations, and effectiveness of the Schiff bases (L1 and L2) and reduced derivatives (L3 and L4) against DNA gyrase B (4PRV) and topoisomerase IV ParE (1S16) proteins. The active sites were examined attentively to enhance result accuracy. Subsequently, the center of the grid box and its dimensions were determined according to binding site residues, providing the entire active site and the full ligand flexibility with additional space, exhibiting strong matching with the extensive evaluations. Table S12 includes the crucial docking parameters of 4PRV (DNA gyrase B) and 1S16 (topoisomerase IV parE). The grid box sizes varied slightly depending on the protein (Table S12). The obtained docking results were visualized using BIOVIA Discovery Studio Visualizer.

DNA gyrase and topoisomerase IV conduct an important chemical reaction known as double-stranded DNA passage. These enzymes are composed of two subunits that share structural similarities, particularly in ATP domains. The DNA gyrase (GyrA and GyrB subunits) mainly

regulates the bacterial genetic material in superhelical form by relaxing positive supercoils (over-winding) and generating negative supercoils (under-winding), which is essential in DNA replication and transcription. The GyrB subunit provides the required energy by breaking down ATP in its active site. Like DNA gyrase, topoisomerase IV consists of ParC (catalytic subunit) and ParE (ATPase subunit). Its primary role is to resolve catenated and knotted DNA from genetic material, managing the failure of cell division. Inhibition of bacterial DNA gyrase prevents the synthesis of DNA and RNA via the inhibition of transcription and replication processes, respectively. The inhibition of topoisomerase mainly leads to stalled or catastrophic cell division (Collins and Osheroff, 2024).

The results of the docking ligand interaction show that L1 forms hydrogen bonds with Asn46, Lys103, and Tyr109 residues through the hydroxyl groups on the aromatic rings, while also interacting with the Glu50 residue via a pi-anion, which is supported by the conjugated system. In addition, aromatic rings and aliphatic carbon moieties in L1 generate hydrophobic contacts with Ile78, Ile94, Tyr109, and Val120, facilitating the creation of a hydrophobic pocket (Fig. 5). L2, similar to L1, makes essential hydrogen bonding interactions through hydroxyl groups. The hydrophobic interaction of L2 includes Pro79 instead of Ile94, which changes the binding mode slightly. The most notable difference is that L2 docking shows an additional amide- π stacking interaction with the Gly117 residue (Fig. 6). The amide- π stacking interactions have been found to play a crucial role in ligand binding and inhibitory activity (de Freitas and Schapira, 2017). Therefore, it can be suggested that this interaction may contribute to the binding affinity of L2 to the protein, which may be one of the reasons for the higher anti-bacterial activity observed experimentally compared to L1. However, the binding energy of L1 ($-7.58 \text{ kcal mol}^{-1}$) was found to be slightly lower than that of L2 ($-7.51 \text{ kcal mol}^{-1}$). The contradiction between interactions and binding energies can be attributed to the AutoDock scoring function, which considers the binding affinities coupled with other contributing factors, like torsional degrees of freedom. The more rotatable bonds increase the flexibility of L2, resulting in a decrease in binding energy.

The docking results for the reduced derivatives indicate that L3 and L4 form hydrogen bonds with the Asn46, Tyr109, and Val120 residues, as well as ionic interactions with Lys103 (Figs. 7 and 8). The observed difference is that L3 engages in a pi-ionic interaction with the Glu50, whereas L4 forms a hydrogen bond with the same residue. Contrary to

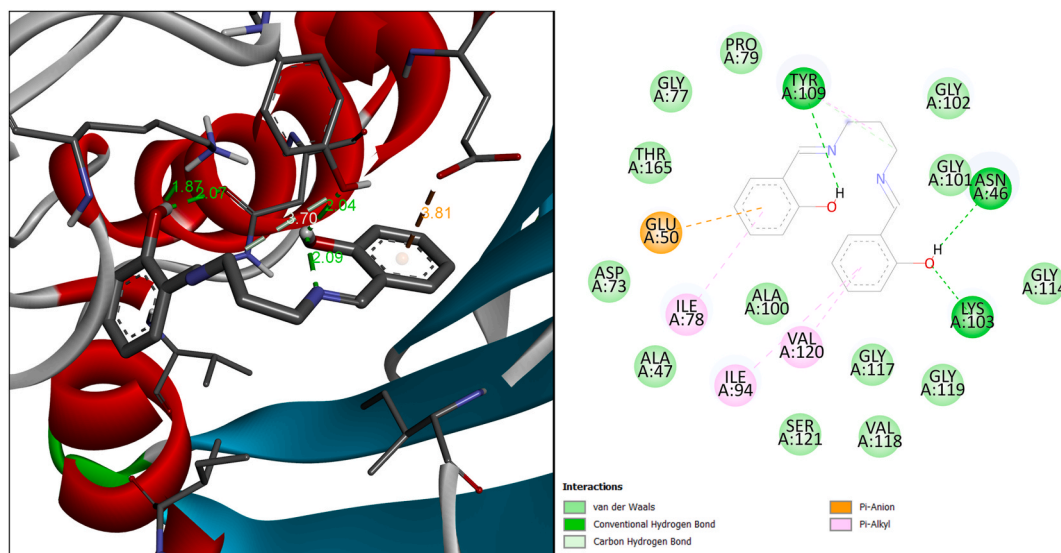


Fig. 5. Docking results of L1 against the DNA gyrase B (4PRV) protein of *E. coli*. The receptor–ligand interaction is represented on a 3D diagram (Left) and a 2D diagram (Right). Conventional hydrogen bond interactions are represented in bright green dotted lines. Pi-anion and Pi-alkyl interactions are shown in orange and pink dotted lines, respectively. (For interpretation of the references to color in this figure legend, the reader is referred to the Web version of this article.)

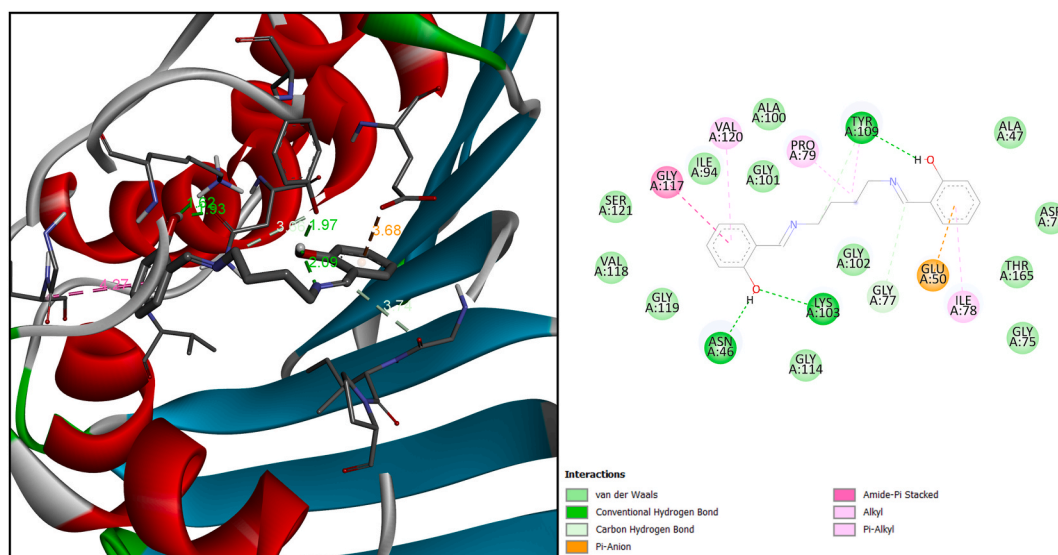


Fig. 6. Docking results of L2 against the DNA gyrase B (4PRV) protein of *E. coli*. The receptor–ligand interaction is represented on a 3D diagram (Left) and a 2D diagram (Right). Conventional hydrogen bond interactions are represented in bright green dotted lines. Amide- π stacked and π -alkyl interactions are shown in dark pink and light pink dotted lines, respectively. (For interpretation of the references to color in this figure legend, the reader is referred to the Web version of this article.)

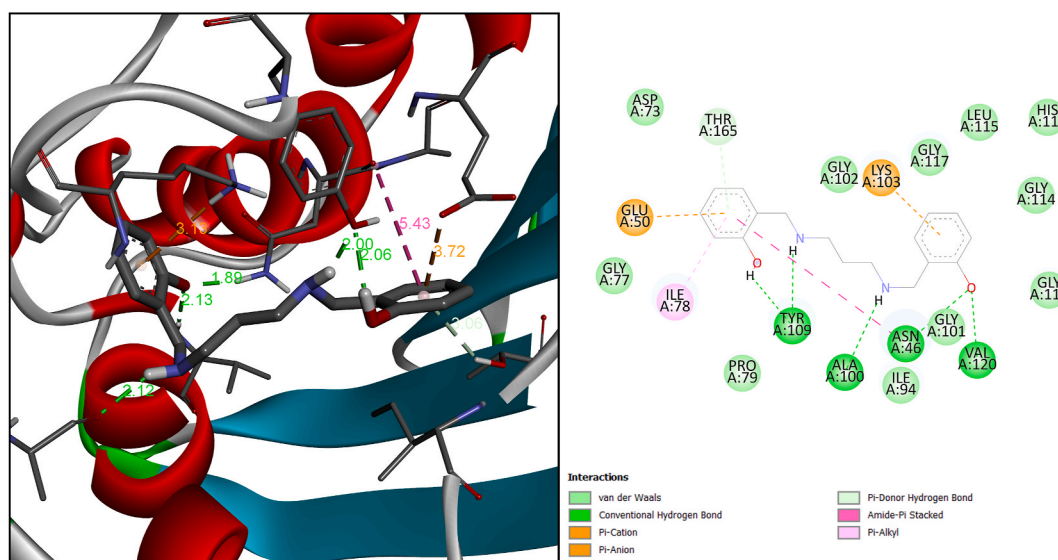


Fig. 7. Docking results of L3 against the DNA gyrase B (4PRV) protein of *E. coli*. The receptor–ligand interaction is represented on a 3D diagram (Left) and a 2D diagram (Right). Conventional hydrogen bond interactions are represented in bright green dotted lines. π -ion, Amide- π stacked and π -alkyl interactions are shown in orange, dark pink and light pink dotted lines, respectively. (For interpretation of the references to color in this figure legend, the reader is referred to the Web version of this article.)

L1 and L2 (Figs. 5 and 6), reduced derivatives (Figs. 7 and 8) construct additional hydrogen bonds with the Ala100 and Tyr109 residues thanks to rotatable amine nitrogen atoms that serve as hydrogen bond donors. Moreover, reduced derivatives also show amide- π stacking through aromatic rings with Asn46, just as observed in the ADP-DNA gyrase B complex, including the π -donor hydrogen bond interaction with Thr165. These additional interactions observed for L3 and L4 can account for their experimentally higher antibacterial activity compared to L1 and L2. Moreover, among the compounds studied, L4 is the only molecule that forms a hydrogen bond with the GLU residue in the DNA gyrase protein. This interaction can be one of the factors contributing to the highest antibacterial activity obtained for L4. The binding energies for L3 ($-7.67 \text{ kcal mol}^{-1}$) and L4 ($-7.84 \text{ kcal mol}^{-1}$) are consistent with the observed trend in experimental inhibition activities. It can be

suggested that L4, having the lowest binding energy, displays the strongest interaction with the active site of DNA gyrase B.

In the interactions of the title molecules with topoisomerase IV, comparable trends to DNA gyrase B were obtained. The main difference observed is that the imine nitrogen atoms of L1 and L2 (Figs. S6 and S7), which act as hydrogen bond acceptors, exhibit hydrogen bond interactions with topoisomerase IV in contrast to DNA gyrase B. The docking results of topoisomerase IV–ligand interaction reveal that all ligands establish hydrogen bonds with the Asn1042 and Tyr1105 residues. Additionally, they engage with Glu1046 through π -anion interactions, assisted by the conjugated system. However, some important differences were observed between the interaction profiles of the ligands. For instance, L1 forms a hydrogen bond with Gly1098 via a single imine nitrogen atom, whereas L2 utilizes both imine nitrogen atoms to

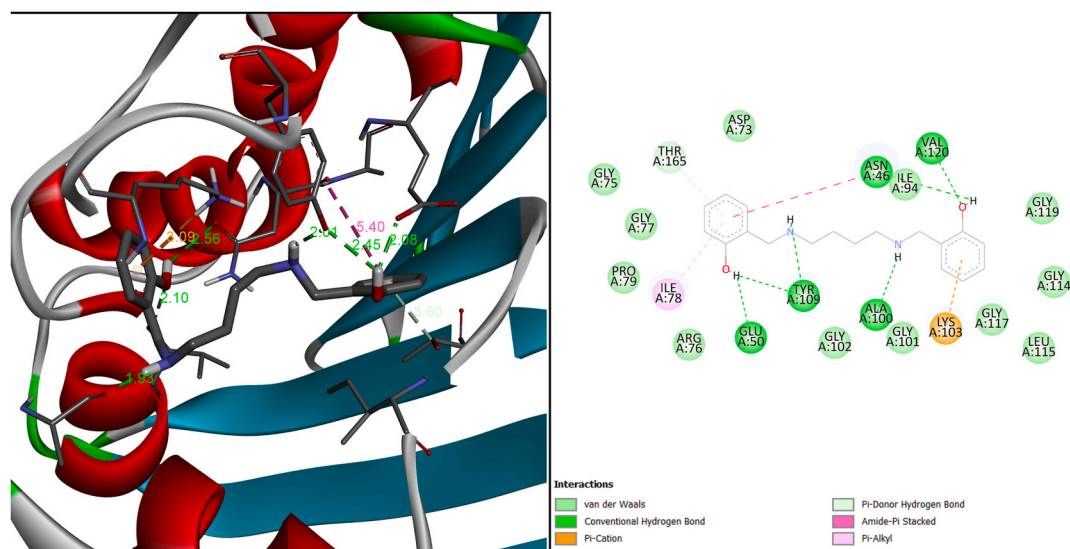


Fig. 8. Docking results of L4 against the DNA gyrase B (4PRV) protein of *E. coli*. The receptor–ligand interaction is represented on a 3D diagram (Left) and a 2D diagram (Right). Conventional hydrogen bond interactions are represented in bright green dotted lines. Pi-cation, Amide-Pi stacked and Pi-alkyl interactions are shown in orange, dark pink and light pink dotted lines, respectively. (For interpretation of the references to color in this figure legend, the reader is referred to the Web version of this article.)

establish hydrogen bonds with Gly1098 and Tyr1105 residues. Aromatic rings and aliphatic carbon moieties support the hydrophobic interactions for the ligands. While L1 creates these hydrophobic contacts with Met1074, Ile1090, and Tyr1105, L2 establishes similar interactions with Pro1075, Ile1090, and Tyr1105.

Similar to DNA gyrase B, the amine nitrogen atoms of reduced derivatives (L3 and L4) act as additional hydrogen bond donors for topoisomerase IV, and pi and hydrophobic interactions contribute to the stabilization of the ligands within a binding pocket (Fig. S8 and S9). The most striking difference between the Schiff bases and the reduced derivatives is that Schiff bases form hydrogen bonds with Lys1099, whereas reduced derivatives construct pi-ion interactions with the same residue via aromatic rings. In addition, the most noticeable difference among all ligands is that L4 is the only molecule that constructs a hydrogen bond with Asp1069, one of the crucial amino acids in the type II topoisomerase ATPase domain for activity.

The binding energy values of ligands in the topoisomerase IV active site exhibited a comparable trend to DNA gyrase B. Similarly to DNA gyrase, L4 has the lowest binding energy ($-7.84 \text{ kcal mol}^{-1}$), while L1 has the highest ($-7.34 \text{ kcal mol}^{-1}$) in the topoisomerase interaction. However, in contrast to DNA gyrase B, L2 exhibits lower binding energy ($-7.71 \text{ kcal mol}^{-1}$) than L3 ($-7.56 \text{ kcal mol}^{-1}$). The fact that the hydrogen bonding between L2 and LYS1099 is relatively strong compared to the pi-ion interaction of L3 with the same residue could be an important factor altering their binding affinities. Although the same pi-ion interaction is valid for L4, the additional hydrogen bond with Asp1069 may have improved its pose in the protein-binding pocket and allowed it to better interact with topoisomerase IV.

In conclusion, molecular docking simulations show that the hydrogen-donating ability of Schiff bases is enhanced by the reduction of imine bonds, which also provides flexibility thanks to the rotatable amine bonds. This computational approach is consistent with experimental findings showing that L4 is a more effective antibacterial agent. The favorable binding of L4 to target proteins can be attributed to its strong hydrogen donor and acceptor capabilities, along with higher flexibility from its extended alkyl chain and rotatable C–N bonds, as discussed in Section 3.2.

3.5. The combined effect of gamma irradiation and antibacterial formulation

Based on the experimental and theoretical findings, L4 was selected as an antimicrobial agent to examine the combined effect of gamma irradiation and antibacterial formulation on the microbial inactivation of the bacteria cocktail. The samples were subjected to low-dose irradiation (1.2 kGy) to obtain countable colonies after the treatments; therefore, the log reduction of the bacteria colonies was determined more precisely. The control sample and reduction of the bacteria colonies after the different treatment processes are shown in Fig. 9. The log value of the control (C) sample was found to be 5.08 CFU mL^{-1} . After the application of the antibacterial formulation (AB) alone, the bacteria colonies reduced to 4.08 CFU mL^{-1} (1 log). The gamma-ray treatment alone showed a similar result. Following the irradiation (GI), the bacteria colonies decreased to 3.82 CFU mL^{-1} , representing a reduction of 1.26 log. However, the combined treatment of gamma irradiation with antimicrobial formulation, regardless of the application sequence (GI + AB or AB + GI), had a marked effect on the reduction of colony number

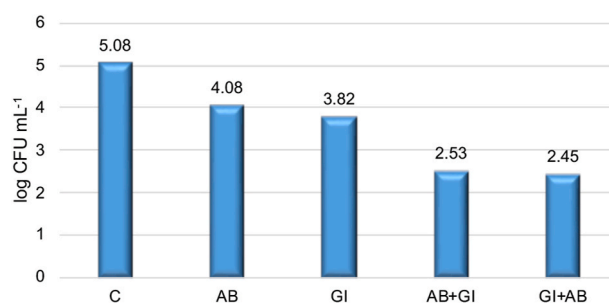


Fig. 9. The individual and combined effects of gamma irradiation and antibacterial formulation. C represents the control sample (non-treated), AB represents the sample treated with the antibacterial formulation (L4) alone, GI represents the sample treated with the gamma irradiation (1.2 kGy) alone, AB + GI represents the sample treated with the antibacterial formulation (L4) followed by gamma irradiation (1.2 kGy), and GI + AB represents the sample treated with the gamma irradiation (1.2 kGy) followed by the antibacterial formulation (L4). The concentration of viable bacterial counts after treatment was expressed as the logarithm of the number of colony-forming units per milliliter ($\log \text{ CFU mL}^{-1}$).

(approximately 2.6 log). These findings indicated that the application of L4 with gamma irradiation increased the radiosensitivity of the bacteria species in the cocktail.

According to inhibition zone studies, L4 has the ability to suppress some mechanisms essential for the growth and survival of the several bacteria present in the cocktail. For instance, the inhibition effect of L4 on DNA gyrase B and topoisomerase IV has been shown by theoretical studies. The primary mechanism of microbial inhibition by ionizing radiation involves the direct disruption of chemical bonds within the DNA molecules or the indirect modification of membrane permeability by oxidative radicals originating from the radiolysis of water (Ji et al., 2022). Accordingly, irradiation can enhance the passage of L4 through the cell membrane, thereby providing contact of more agent molecules with the target. In addition, the direct damage caused by the radiation cannot be repaired due to the inhibitory effect of L4 on the specific enzymes involved in the repair process.

It should be noted that a reduction of 2.6 log bacteria was obtained for heavily contaminated samples (bacteria cocktail) irradiated at a low dose (1.2 kGy). However, most textile artifacts do not contain such a high microbial load. Therefore, the decontamination dose for the combined treatment can be selected according to the microbial load on the textile article concerned.

Previous studies have demonstrated that the combination of ionizing radiation and antibacterial agents is an effective method for food preservation (Balaji et al., 2022; Begum et al., 2022; Ji et al., 2021, 2022; Shankar et al., 2022; Ben-Fadhel et al., 2021; Hossain et al., 2021; Robichaud et al., 2021; Zhang et al., 2020; Berdejo et al., 2019; Tawema et al., 2016). For instance, Balaji et al. (2022) reported that the initial content of sporulated *B. cereus* was 6.25 log CFU mL⁻¹, after the irradiation treatment at 5 kGy without antimicrobial formulation, a value of 3.64 log CFU mL⁻¹ was found. However, the combined treatment of formulations 1 and 2 with the gamma irradiation at 5 kGy reduced *B. cereus* by 1.25 and 1.19 log CFU mL⁻¹, respectively. The formulations 3 and 4 resulted in a complete inactivation of *B. cereus* spores. However, regarding the cultural heritage field, there has been a limited number of studies examining the application of gamma irradiation with antimicrobial agents. Sakr et al. (2019) showed the use of triclazole at a concentration of 10 µg mL⁻¹ in DMSO completely inhibited melanin production caused by *Streptomyces* spp. isolated from some ancient Egyptian tombs after gamma irradiation at sub-lethal doses. Petushkova and Koestler (1996) reported the decontamination effect of gamma irradiation at doses of 2.5–5.0 kGy combined with a pretreatment of 3 % Catamin AB on bacilli. Capraru et al. (2022) showed the efficiency of the combined treatment on the new cotton textile materials. It was reported that the application of Ag/chitosan combined with gamma irradiation demonstrated a significant impact on *Staphylococcus aureus* compared to the control, resulting in inhibition zones of 9–10 mm. The scope of these investigations have largely been confined to a limited number of microbial species. Our research significantly expands this scope by being the first, to our knowledge, that comprehensively evaluates the combined effect of gamma irradiation and a green antibacterial agent against the microbial cocktail. As real-world contamination in artifacts involves complex microbial communities rather than single strains, the present study provides a more realistic, applicable, and environmentally friendly solution for the decontamination of valuable cultural heritage.

As a result, this combined application can be suggested as a promising technique for reducing the required dose for the microbial decontamination of artifacts. In the subsequent phase, research will be performed to ensure that this application does not harm the structural integrity and color of textile artifacts.

4. Conclusion

The present study is designed to investigate the combination of antimicrobial agents with ionizing radiation to reduce the required dose to inactivate the microorganisms on historical textiles. Assuming a

worst-case scenario in which a textile artifact is contaminated with most of the microorganisms present in the museum, cocktails of bacteria and mold species isolated from all possible areas were prepared and exposed to gamma radiation at different doses. According to the survivors versus dose plot, the mean doses of 7.60 and 6.32 kGy were found to be the required doses for complete inactivation of the bacteria and mold cocktail, respectively. These doses can cause unwanted side effects on some textile artifacts. Concerning the minimization of the required dose, two Schiff bases (L1 and L2) and their reduced forms (L3 and L4) were prepared, and their antimicrobial activity against gamma-resistant microorganism colonies was investigated. The synthesized molecules showed antibacterial activity. The microbiological studies and theoretical approaches revealed that the reduction of the imine bond positively influences antibacterial activity by enhancing the hydrogen bond donation ability of the molecules. According to molecular docking studies, L4, a reduced derivative with high flexibility and dipole moment, showed the greatest binding affinity to the active site of DNA gyrase B and topoisomerase IV. Therefore, L4, as the most promising antibacterial agent among the title compounds, was tested to examine the combined effect of the antibacterial agent and gamma irradiation. This combined treatment showed strong inhibition on the bacteria cocktail. This research proposed an alternative approach for preserving the historical textiles. However, future studies are planned to determine the effect of L4 on the quality of textile artifacts.

CRedit authorship contribution statement

Ece Ergun: Writing – original draft, Project administration, Investigation, Formal analysis, Conceptualization. **Hilal B.D. Halkman:** Writing – review & editing, Methodology, Formal analysis, Data curation. **Eren Kasımırtuna:** Writing – review & editing, Visualization, Software, Methodology, Data curation. **Ömer Kantoğlu:** Writing – review & editing, Resources, Conceptualization. **Ümit Ergun:** Writing – review & editing, Supervision, Software, Investigation. **Ersin Orhan:** Writing – review & editing, Resources, Formal analysis.

Declaration of competing interest

The authors declare that they have no known competing financial interests or personal relationships that could have appeared to influence the work reported in this paper.

Acknowledgements

This study has been supported by the International Atomic Energy Agency (IAEA) through the project on Development and Implementation of Cultural Heritage Preservation Using Ionizing Radiation Technology (F22082-CRP-26647) and the Turkish Energy, Nuclear, and Mineral Research Agency (TENMAK) through Provision of Measurement, Analysis, Testing, Irradiation, and Calibration Services and Development of Measurement Capabilities (A4.H1.F24).

Appendix A. Supplementary data

Supplementary data to this article can be found online at <https://doi.org/10.1016/j.radphyschem.2025.113247>.

Data availability

Data will be made available on request.

References

- Abdel-Halim, M.E.F., Ali, M.F., Ghaly, M.F., Sakr, A.A., 2013. Efficiency of antibiotics and gamma irradiation in eliminating streptomyces strains isolated from paintings of ancient Egyptian tombs. *J. Cult. Herit.* 14, 45–50. <https://doi.org/10.1016/j.culher.2012.03.009>.

- Agu, P.C., Afikwa, C.A., Orji, O.U., Ezech, E.M., Ofoke, I.H., Ogbu, C.O., Ugwuja, E.I., Aja, P.M., 2023. Molecular docking as a tool for the discovery of molecular targets of nutraceuticals in diseases management. *Sci. Rep.* 13, 1–18. <https://doi.org/10.1038/s41598-023-40160-2>.
- Ahmad, I., Kuznetsov, A.E., Pirzada, A.S., Alsharif, K.F., Daglia, M., Khan, H., 2023. Computational pharmacology and computational chemistry of 4-hydroxyisoleucine: physicochemical, pharmacokinetic, and DFT-based approaches. *Front. Chem.* 11, 1145974. <https://doi.org/10.3389/fchem.2023.1145974>.
- Akbari, Z., Stagno, C., Iraci, N., Efferth, T., Omer, E.A., Piperno, A., Montazerohori, M., Feizi-Dehmayebi, M., Micale, N., 2024. Biological evaluation, DFT, MEP, HOMO-LUMO analysis and ensemble docking studies of Zn(II) complexes of bidentate and tetradentate Schiff base ligands as antileukemia agents. *J. Mol. Struct.* 1301, 137400. <https://doi.org/10.1016/j.molstruc.2023.137400>.
- Ateş, B.M., Zeybek, B., Aksu, M., Ergun, Ü., Ercean, F., Aksu, M.L., Atakol, O., 2010. Thermal decomposition of new mononuclear Ni^{II} complexes with ONNO type reduced schiff bases and pseudo halogens. *Z. Anorg. Allg. Chem.* 636, 840–845. <https://doi.org/10.1002/zaac.200900499>.
- Balaji, A.S., Allahdad, Z., Lacroix, M., 2022. Effect of γ -irradiation in combination with natural antimicrobial formulation on microbial inactivation, protein digestibility and quality of mothers' milk. *Int. Dairy J.* 131, 105386. <https://doi.org/10.1016/j.idairyj.2022.105386>.
- Barone, V., Cossi, M., 1998. Quantum calculation of molecular energies and energy gradients in solution by a conductor solvent model. *J. Phys. Chem. A* 102, 1995–2001. <https://doi.org/10.1021/jp9716997>.
- Begum, T., Follett, P.A., Mahmud, J., Moskovchenko, L., Salmieri, S., Allahdad, Z., Lacroix, M., 2022. Silver nanoparticles-essential oils combined treatments to enhance the antibacterial and antifungal properties against foodborne pathogens and spoilage microorganisms. *Microb. Pathog.* 164, 105411. <https://doi.org/10.1016/j.micpath.2022.105411>.
- Bellon, S., Parsons, J.D., Wei, Y., Hayakawa, K., Swenson, L.L., Charifson, P.S., Lippke, J.A., Aldape, R., Gross, C.H., 2004. Crystal structures of escherichia coli topoisomerase IV ParE subunit (24 and 43 Kilodaltons): a single residue dictates differences in novobiocin potency against topoisomerase IV and DNA gyrase. *Antimicrob. Agents Chemother.* 48, 1856–1864. <https://doi.org/10.1128/AAC.48.5.1856-1864.2004>.
- Ben-Fadhel, Y., Cingolani, M.C., Li, L., Chazot, G., Salmieri, S., Horak, C., Lacroix, M., 2021. Effect of γ -irradiation and the use of combined treatments with edible bioactive coating on carrot preservation. *Food Packag. Shelf Life* 28, 100635. <https://doi.org/10.1016/j.foodpack.2021.100635>.
- Berdejo, D., Pagán, E., García-Gonzalo, D., Pagán, R., 2019. Exploiting the synergism among physical and chemical processes for improving food safety. *Curr. Opin. Food Sci.* 30, 14–20. <https://doi.org/10.1016/j.cofs.2018.08.004>.
- Bhatia, M., 2024. An overview of conceptual-DFT based insights into global chemical reactivity of volatile sulfur compounds (VSCs). *Comput. Toxicol.* 29, 100295. <https://doi.org/10.1016/j.comtox.2023.100295>.
- Branysova, T., Demnerova, K., Durovic, M., Stiborova, H., 2022. Microbial biodeterioration of cultural heritage and identification of the active agents over the last two decades. *J. Cult. Herit.* 55, 245–260. <https://doi.org/10.1016/j.culher.2022.03.013>.
- Capraru, O.-A., Lungu, B., Virgolici, M., Constantin, M., Cutrubinis, M., Chirila, L., Cinteza, L.O., Stanculescu, I., 2022. Gamma irradiation and Ag and ZnO nanoparticles combined treatment of cotton textile materials. *Materials* 15, 2734. <https://doi.org/10.3390/ma15082734>.
- Caron, G., Digiesi, V., Solaro, S., Ermondì, G., 2020. Flexibility in early drug discovery: focus on the beyond-Rule-of-5 chemical space. *Drug Discov. Today* 25, 621–627. <https://doi.org/10.1016/j.drudis.2020.01.012>.
- Ceramella, J., Iacopetta, D., Catalano, A., Cirillo, F., Lappano, R., Sinicropi, M.S., 2022. A review on the antimicrobial activity of schiff bases: data collection and recent studies. *Antibiotics* 11, 191. <https://doi.org/10.3390/antibiotics11020191>.
- Chirila, L., Popescu, A., Cutrubinis, M., Stanculescu, I., Moise, V.I., 2018. The influence of gamma irradiation on natural dyeing properties of cotton and flax fabrics. *Radiat. Phys. Chem.* 145, 97–103. <https://doi.org/10.1016/j.radphyschem.2017.12.017>.
- Chohan, Z.H., Arif, M., Rashid, A., 2008. Copper (II) and zinc (II) metal based salicyl-, furanyl-, thienyl- and pyrrolyl-derived ONNO, NNNO, ONNS & NNNS donor asymmetrically mixed schiff-bases with antibacterial and antifungal potentials. *J. Enzym. Inhib. Med. Chem.* 23, 785–796. <https://doi.org/10.1080/14756360701450145>.
- Cirone, M., Figoli, A., Galiano, F., La Russa, M.F., Macchia, A., Mancuso, R., Ricca, M., Rovella, N., Taverniti, M., Ruffolo, S.A., 2023. Innovative methodologies for the conservation of cultural heritage against biodeterioration: a review. *Coatings* 13, 1986. <https://doi.org/10.3390/coatings13121986>.
- Collins, J.A., Osheroff, N., 2024. Gyrase and topoisomerase IV: recycling old targets for new antibacterials to combat fluoroquinolone resistance. *ACS Infect. Dis.* 10, 1097–1115. <https://doi.org/10.1021/acsinfecdis.4c00128>.
- Danyo, E.K., Ivantsova, M.N., Selezneva, I.S., 2024. Ionizing radiation effects on microorganisms and its applications in the food industry. *Foods Raw Mater* 12, 1–12. <https://doi.org/10.21603/2308-4057-2024-1-583>.
- Darlam, J., Sharma, S., 2024. The role of physicochemical and topological parameters in drug design. *Front. Drug Discov.* 4, 1424402. <https://doi.org/10.3389/fddsv.2024.1424402>.
- de Freitas, R.F., Schapira, M., 2017. A systematic analysis of atomic protein–ligand interactions in the PDB. *Med. Chem. Commun.* 8, 1970. <https://doi.org/10.1039/C7MD00381A>.
- Di Carlo, E., Chisesi, R., Barresi, G., Barbaro, S., Lombardo, G., Rotolo, V., Sebastianelli, M., Travagliato, G., Palla, F., 2016. Fungi and bacteria in indoor cultural Heritage environments: Microbial-Related risks for artworks and human health. *Environ. Ecol. Res.* 4, 257–264. <https://doi.org/10.13189/eer.2016.040504>.
- Filarowski, A., Głowiaka, T., Koll, A., 1999. Strengthening of the intramolecular O...H...N hydrogen bonds in schiff bases as a result of steric repulsion. *J. Mol. Struct.* 484, 75–89. [https://doi.org/10.1016/S0022-2860\(98\)00660-7](https://doi.org/10.1016/S0022-2860(98)00660-7).
- Forlani, G., Seves, A.M., Ciferri, O., 2000. A bacterial extracellular proteinase degrading silk fibroin. *Int. Biodeterior. Biodegrad.* 46, 271–275. [https://doi.org/10.1016/S0964-8305\(00\)00099-8](https://doi.org/10.1016/S0964-8305(00)00099-8).
- Gogoi, H.P., Barman, P., 2023. Salophen type ONNO donor schiff base complexes: synthesis, characterization, bioactivity, computational, and molecular docking investigation. *Inorg. Chim. Acta.* 556, 121668. <https://doi.org/10.1016/j.ica.2023.121668>.
- Grimme, S., Ehrlich, S., Goerigk, L., 2011. Effect of the damping function in dispersion corrected density functional theory. *J. Comput. Chem.* 32, 1456–1465. <https://doi.org/10.1002/jcc.21759>.
- Guex, N., Peitsch, M.C., 1997. Swiss PDB viewer - references. *Electrophoresis* 18.
- Gutarowska, B., Pietrzak, K., Machnowski, W., Miczarek, J.M., 2017. Historical textiles—a review of microbial deterioration analysis and disinfection methods. *Textil. Res. J.* 87, 2388–2404. <https://doi.org/10.1177/0040517516669076>.
- Hanwell, M.D., Curtis, D.E., Lonie, D.C., Vandermeersch, T., Zurek, E., Hutchison, G.R., 2016. Avogadro: an open-source Molecular Builder and Visualization Tool. *Comput. Phys. Commun.* 178, 226–240. <https://doi.org/10.1016/j.cpc.2015.08.032>.
- Hanwell, M.D., Curtis, D.E., Lonie, D.C., Vandermeersch, T., Zurek, E., Hutchison, G.R., 2012. Avogadro: an advanced semantic chemical editor, visualization, and analysis platform. *J. Cheminf.* 4, 17. <https://doi.org/10.1186/1758-2946-4-17>.
- Hossain, F., Follett, P., Shankar, S., Begum, T., Salmieri, S., Lacroix, M., 2021. Radiosensitization of rice weevil Sitophilus oryzae using combined treatments of essential oils and ionizing radiation with gamma-ray and X-Ray at different dose rates. *Radiat. Phys. Chem.* 180, 109286. <https://doi.org/10.1016/j.radphyschem.2020.109286>.
- International Atomic Energy Agency, 2017. Uses of Ionizing Radiation for Tangible Cultural Heritage Conservation. IAEA Radiation Technology Series No. 6. IAEA, Vienna.
- Ji, J., Shankar, S., Fernandez, J., Juillet, E., Salmieri, S., Lacroix, M., 2021. A rapid way of formulation development revealing potential synergic effects on numerous antimicrobial combinations against foodborne pathogens. *Microb. Pathog.* 158, 105047. <https://doi.org/10.1016/j.micpath.2021.105047>.
- Ji, J., Shankar, S., Salmieri, S., Lacroix, M., 2022. Combined effects of microencapsulated essential oils and γ -irradiation on microbiological and physicochemical properties of dry fermented sausages during ripening and storage. *Food Control* 133, 108624. <https://doi.org/10.1016/j.foodcont.2021.108624>.
- Kantoglu, Ö., Ergun, E., Ozmen, D., Halkman, H.B.D., 2018. A biological survey on the ottoman archive papers and determination of the D10 value. *Radiat. Phys. Chem.* 144, 204–210. <https://doi.org/10.1016/j.radphyschem.2017.08.016>.
- Kargar, H., Fallah-Mehrjardi, M., Behjatmanesh-Ardakani, R., Rudbari, H.A., Ardakani, A.A., Sedighi-Khavidak, S., Munawar, K.S., Ashfaq, M., Tahir, M.N., 2022. Synthesis, spectral characterization, crystal structures, biological activities, theoretical calculations and substitution effect of salicylidene ligand on the nature of mono and dinuclear Zn(II) schiff base complexes. *Polyhedron* 213, 115636. <https://doi.org/10.1016/j.poly.2021.115636>.
- Kavkler, K., Gunde-Cimerman, N., Zalar, P., Demšar, A., 2015. Fungal contamination of textile objects preserved in Slovene museums and religious institutions. *Int. Biodeterior. Biodegrad.* 97, 51–59. <https://doi.org/10.1016/j.ibiod.2014.09.020>.
- Kavkler, K., Pucić, I., Zalar, P., Demšar, A., Mihaljević, B., 2018. Is it safe to irradiate historic silk textile against fungi? *Radiat. Phys. Chem.* 150, 101–110. <https://doi.org/10.1016/j.radphyschem.2018.04.030>.
- Li, S., Zhang, G., Zhou, Y., Sun, H., Yan, L., Feng, X., Li, L., 2025. Exploring the feasibility of low energy electron beam irradiation decontamination for textile cultural heritage. *npj Herit. Sci.* 13, 271. <https://doi.org/10.1038/s40494-025-01837-1>.
- Lipinski, C.A., Lombardo, F., Dominy, B.W., Feeney, P.J., 1997. Experimental and computational approaches to estimate solubility and permeability in drug discovery and development settings. *Adv. Drug Deliv. Rev.* 23, 3–25. [https://doi.org/10.1016/S0169-409X\(96\)00423-1](https://doi.org/10.1016/S0169-409X(96)00423-1).
- Marušić, K., Klarić, M.S., Sincić, L., Pucić, I., Mihaljević, B., 2020. Combined effects of gamma-irradiation, dose rate and mycobiota activity on cultural heritage – study on model paper. *Radiat. Phys. Chem.* 170, 108641. <https://doi.org/10.1016/j.radphyschem.2019.108641>.
- Mazzoli, R., Giuffrida, M.G., Pessione, E., 2018. Back to the past: “find the guilty bug—microorganisms involved in the biodeterioration of archeological and historical artifacts”. *Appl. Microbiol. Biotechnol.* 102, 6393–6407. <https://doi.org/10.1007/s00253-018-9113-3>.
- Morris, G.M., Ruth, H., Lindstrom, W., Sanner, M.F., Bewley, R.K., Goodsell, D.S., Olson, A.J., 2009. Software news and updates AutoDock4 and AutoDockTools4: automated docking with selective receptor flexibility. *J. Comput. Chem.* 30, 2785–2791. <https://doi.org/10.1002/jcc.21256>.
- Musatat, A.B., Durmuş, T., Atahan, A., 2024. Harnessing high potential benzothiazole chalcones against dengue virus NS5 protein: a multi-faceted theoretical study through molecular docking, ADME, and DFT. *Arch. Biochem. Biophys.* 761, 110171. <https://doi.org/10.1016/j.abb.2024.110171>.
- Mushtaq, I., Ahmad, M., Saleem, M., Ahmed, A., 2024. Pharmaceutical significance of schiff bases: an overview. *Futur. J. Pharm. Sci.* 10, 16. <https://doi.org/10.1186/s43094-024-00594-5>.
- Neese, F., 2022. Software update: the ORCA program system—Version 5.0. *Wiley Interdiscip. Rev. Comput. Mol. Sci.* 12, 1–15. <https://doi.org/10.1002/wcms.1606>.
- Oboňová, B., Habala, L., Litecká, M., Herich, P., Bilková, A., Bilka, F., Horváth, B., 2023. Antimicrobially active Zn(II) complexes of reduced schiff bases derived from cyclohexane-1,2-diamine and fluorinated benzaldehydes—synthesis, crystal structure and bioactivity. *Life* 13, 1516. <https://doi.org/10.3390/life13071516>.

- Pandey, R., Gupta, V., Pandit, P., Rohit, K., Pandey, S., 2022. Textile intangible cultural heritage of the world. In: Jose, S., Thomas, S., Pandit, P., Pandey, R., Gupta, V. (Eds.), *Handbook of Museum Textiles*. Scrivener Publishing LLC, MA, pp. 19–37. <https://doi.org/10.1002/9781119983903.ch2>.
- Persistence of Vision Raytracer Pty. Ltd., 2013a. POV-Ray for Windows Editor DLL, Version 3.7.
- Persistence of Vision Raytracer Pty. Ltd., 2013b. POV-Ray: Persistence of Vision Raytracer.
- Petersen, E.F., Goddard, T.D., Huang, C.C., Couch, G.S., Greenblatt, D.M., Meng, E.C., Ferrin, T.E., 2004. UCSF Chimera - a visualization system for exploratory research and analysis. *J. Comput. Chem.* 25, 1605–1612. <https://doi.org/10.1002/jcc.20084>.
- Petushkova, J.P., Koestler, R.J., 1996. Biodeterioration studies on parchment and leather attacked by bacteria in the Commonwealth of socialist states. In: *International Conference on Conservation and Restoration of Archival and Library Materials*, vol. 1, pp. 195–211. Erice.
- Pinzi, L., Rastelli, G., 2019. Molecular docking: shifting paradigms in drug discovery. *Int. J. Mol. Sci.* 20, 4331. <https://doi.org/10.3390/ijms20184331>.
- Ponta, C.C., Havermans, J.B.G.A., Boutaine, J.L., 2017. Disinfection of cultural artefacts using irradiation. In: *IAEA. Uses of Ionizing Radiation for Tangible Cultural Heritage Conservation*. IAEA, Vienna, Austria, pp. 93–103.
- Reglinski, J., Morris, S., Stevenson, D.E., 2002. Supporting conformational change at metal centres. Part 2: four and five coordinate geometry. *Polyhedron* 21, 2175–2182. [https://doi.org/10.1016/S0277-5387\(02\)01172-5](https://doi.org/10.1016/S0277-5387(02)01172-5).
- Richard, A.M., Huang, R., Waidyanatha, S., Shinn, P., Collins, B.J., Thillainadarajah, I., Grulke, C.M., Williams, A.J., Lougee, R.R., Judson, R.S., Houck, K.A., Shobair, M., Yang, C., Rathman, J.F., Yasgar, A., Fitzpatrick, S.C., Simeonov, A., Thomas, R.S., Crofton, K.M., Paules, R.S., Bucher, J.R., Austin, C.P., Kavlock, R.J., Tice, R.R., 2021. The Tox21 10K compound library: collaborative chemistry advancing toxicology. *Chem. Res. Toxicol.* 34, 189–216. <https://doi.org/10.1021/acs.chemrestox.0c00264>.
- Robichaud, V., Bagheri, L., Salmieri, S., Aguilar-Uscanga, B.R., Millette, M., Lacroix, M., 2021. Effect of γ -irradiation and food additives on the microbial inactivation of foodborne pathogens in infant formula. *LWT* 139, 110547. <https://doi.org/10.1016/j.lwt.2020.110547>.
- Roney, M., Singh, G., Dubey, A., Soni, H., Tandon, S., Narasimhaji, C.V., Tufail, A., Akm, M.H., Aluwi, M.F.F.M., 2023. Polypharmacological assessment of Amoxicillin and its analogues against the bacterial DNA gyrase B using molecular docking, DFT and molecular dynamics simulation. *ASP. Mol. Med.* 2, 100024. <https://doi.org/10.1016/j.amolm.2023.100024>.
- Russo, R., Palla, F., 2023. Plant essential oils as biocides in sustainable strategies for the conservation of cultural Heritage. *Sustainability* 15, 8522. <https://doi.org/10.3390/su15118522>.
- Sahu, D., Rathor, L.S., Dwivedi, S.D., Shah, K., Chauhan, N.S., Singh, M.R., Singh, D.A., 2024. Review on molecular docking as an interpretative tool for molecular targets in disease management. *Assay Drug Dev. Technol.* 22, 40–50. <https://doi.org/10.1089/adt.2023.060>.
- Sakr, A.A., Ghaly, M.F., Edwards, H.G.M., Elbashar, Y.H., 2019. Gamma-radiation combined with tricycloazole to protect tempera paintings in ancient Egyptian tombs (Nile Delta, Lower Egypt). *J. Radioanal. Nucl. Chem.* 321, 263–276. <https://doi.org/10.1007/s10967-019-06580-z>.
- Santos-Martins, D., Solis-Vasquez, L., Tillack, A.F., Sanner, M.F., Koch, A., Forli, S., 2021. Accelerating auto dock 4 with GPUs and gradient-based local search. *J. Chem. Theor. Comput.* 17, 1060–1073. <https://doi.org/10.1021/acs.jctc.0c01006>.
- Schaeffer, L., 2008. The role of functional groups in drug–receptor interactions. In: Wermuth, C.G. (Ed.), *The Practice of Medicinal Chemistry*, third ed. Academic Press, San Diego, pp. 464–480. <https://doi.org/10.1016/B978-0-12-374194-3.00021-4>.
- Shankar, S., Karboune, S., Salmieri, S., Lacroix, M., 2022. Development of antimicrobial formulation based on essential oils and gamma irradiation to increase the shelf life of boneless chicken thighs. *Radiat. Phys. Chem.* 192, 109893. <https://doi.org/10.1016/j.radphyschem.2021.109893>.
- Sharma, M., Joshi, P., Kumar, N., Joshi, S., Rohilla, R.K., Roy, N., Rawat, D.S., 2011. Synthesis, antimicrobial activity and structure–activity relationship study of N,N-dibenzyl-cyclohexane-1,2-diamine derivatives. *Eur. J. Med. Chem.* 46, 480–487. <https://doi.org/10.1016/j.ejmech.2010.11.027>.
- Skóra, J., Gutarowska, B., Pielech-Przybylska, K., Stepien, Ł., Pietrzak, K., Piotrowska, M., Pietrowski, P., 2015. Assessment of microbiological contamination in the work environments of museums, archives and libraries. *Aerobiologia* 31, 389–401. <https://doi.org/10.1007/s10453-015-9372-8>.
- Stanger, F.V., Dehio, C., Schirmer, T., 2014. Structure of the N-Terminal gyrase B fragment in complex with ADP-Pi reveals rigid-body motion induced by ATP hydrolysis. *PLoS One* 9, e107289. <https://doi.org/10.1371/journal.pone.0107289>.
- Storer, M.C., Hunter, C.A., 2022. Quantification of secondary electrostatic interactions in H-bonded complexes. *Phys. Chem. Chem. Phys.* 24, 18124–18132. <https://doi.org/10.1039/D2CP03004G>.
- Szostak-Kotow, J., 2004. Biodeterioration of textiles. *Int. Biodeterior. Biodegrad.* 53, 165–170. [https://doi.org/10.1016/S0964-8305\(03\)00090-8](https://doi.org/10.1016/S0964-8305(03)00090-8).
- Tanvir, R., Ijaz, S., Sajid, I., Hasnain, S., 2024. Multifunctional in vitro, in silico and DFT analyses on antimicrobial BagremycinA biosynthesized by *Micromonospora chokoriensis* CR3 from *Hieracium canadense*. *Sci. Rep.* 14, 10976. <https://doi.org/10.1038/s41598-024-61490-9>.
- Tawema, P., Han, J., Vu, K.D., Salmieri, S., Lacroix, M., 2016. Antimicrobial effects of combined UV-C or gamma radiation with natural antimicrobial formulations against *Listeria monocytogenes*, *Escherichia coli* O157: H7, and total yeasts/molds in fresh cut cauliflower. *LWT* 65, 451–456. <https://doi.org/10.1016/j.lwt.2015.08.016>.
- Vujcic, I., Masic, S., Medic, M., Milicevic, B., Dramicanin, M., 2019. The influence of gamma irradiation on the color change of wool, linen, silk, and cotton fabrics used in cultural heritage artifacts. *Radiat. Phys. Chem.* 156, 307–313. <https://doi.org/10.1016/j.radphyschem.2018.12.001>.
- Weigend, F., 2006. Accurate coulomb-fitting basis sets for H to Rn. *Phys. Chem. Chem. Phys.* 8, 1057–1065. <https://doi.org/10.1039/b515623h>.
- Weigend, F., Ahlrichs, R., 2005. Balanced basis sets of split valence, triple zeta valence and quadruple zeta valence quality for H to Rn: design and assessment of accuracy. *Phys. Chem. Chem. Phys.* 7, 3297–3305. <https://doi.org/10.1039/b508541a>.
- Xiong, G., Wu, Z., Yi, J., Fu, L., Yang, Z., Hsieh, C., Yin, M., Zeng, X., Wu, C., Lu, A., Chen, X., Hou, T., Cao, D., 2021. ADMETlab 2.0: an integrated online platform for accurate and comprehensive predictions of ADMET properties. *Nucleic Acids Res.* 49, W5–W14. <https://doi.org/10.1093/nar/gkab255>.
- Zhang, H., Tikekar, R.V., Ding, Q., Gilbert, A.R., Wimsatt, S.T., 2020. Inactivation of foodborne pathogens by the synergistic combinations of food processing technologies and food-grade compounds. *Compr. Rev. Food Sci. Food Saf.* 19, 2110–2138. <https://doi.org/10.1111/1541-4337.12582>.